

1 **Nitrogen demand, availability, and acquisition strategy control plant responses to elevated
2 CO₂**

3

4 Evan A. Perkowski^{1,*}, Ezinwanne Ezekannagha¹, Nicholas G. Smith¹

5 ¹Department of Biological Sciences, Texas Tech University, Lubbock, TX

6

7 *Corresponding author:

8 2901 Main St.

9 Lubbock, TX, 79409

10 Email: evan.a.perkowski@ttu.edu

11

12 **ORCIDs**

13 Evan A. Perkowski (0000-0002-9523-8892)

14 Ezinwanne Ezekannagha (0000-0001-7469-949X)

15 Nicholas G. Smith (0000-0001-7048-4387)

16

17 Total word count: 7284

18 - Introduction: 1420

19 - Methods: 2589

20 - Results: 1069

21 - Discussion: 2206

22

23 Tables: 3

24 Figures: 4

25 Supporting Information: 7 tables, 7 figures

26

27 **Abstract**
28 Plants respond to elevated atmospheric CO₂ concentrations by reducing leaf nitrogen content and
29 photosynthetic capacity – patterns that correspond with increased net photosynthesis and growth.
30 Despite the longstanding notion that nitrogen availability regulates these responses, eco-
31 evolutionary optimality theory posits that changes in leaf nitrogen demand due to elevated CO₂
32 optimize resource allocation to photosynthetic capacity and maximize allocation to growth,
33 independent of nitrogen availability. Here, we examined leaf and whole-plant responses of
34 *Glycine max* L. (Merr) subjected to full-factorial combinations of two CO₂, two inoculation, and
35 nine nitrogen fertilization treatments. Nitrogen fertilization and inoculation did not modify leaf
36 photosynthetic responses to elevated CO₂. Instead, elevated CO₂ decreased the maximum rate of
37 Rubisco carboxylation more strongly than it decreased the maximum rate of electron transport
38 for RuBP regeneration, increasing net photosynthesis by allowing rate-limiting steps to approach
39 optimal coordination. Increasing fertilization enhanced positive whole-plant responses to
40 elevated CO₂ due to increased nitrogen uptake. Inoculation with symbiotic nitrogen-fixing
41 bacteria did not influence leaf or whole-plant responses to elevated CO₂. These results reconcile
42 the role of nitrogen availability and demand on plant responses to elevated CO₂, showing that
43 leaf photosynthetic responses are regulated by changes in leaf nitrogen demand, while whole-
44 plant responses are constrained by nitrogen availability.

45
46 **Summary**
47 Changes in leaf nitrogen demand drove leaf photosynthetic responses to elevated CO₂
48 independent of nitrogen fertilization. Nitrogen fertilization enhanced whole-plant responses to
49 elevated CO₂, while symbiotic nitrogen fixation had no impact on leaf or whole-plant responses
50 to elevated CO₂.

51
52 **Keywords**
53 acclimation, biomass, eco-evolutionary optimality, growth chamber, least-cost theory, nitrogen
54 acquisition strategy, photosynthesis, plant functional ecology
55

56 **Introduction**

57 Complex carbon and nitrogen cycles regulate terrestrial ecosystems. Terrestrial biosphere models
58 that incorporate coupled carbon and nitrogen cycles must accurately represent the processes
59 governing these cycles across varying environmental scenarios in order to reliably simulate
60 carbon and nitrogen fluxes (Hungate *et al.*, 2003; Prentice *et al.*, 2015; Davies-Barnard *et al.*,
61 2020; Kou-Giesbrecht *et al.*, 2023). While the inclusion of these coupled cycles was intended to
62 improve model reliability, uncertainties remain regarding the effects of nitrogen availability and
63 acquisition strategy on leaf and whole-plant responses to increasing atmospheric CO₂
64 concentrations (Davies-Barnard *et al.*, 2020, 2022). These uncertainties contribute to divergent
65 predictions of future carbon and nitrogen flux simulations across models (Friedlingstein *et al.*,
66 2014; Wieder *et al.*, 2015; Arora *et al.*, 2020; Meyerholt *et al.*, 2020).

67 Research over the past few decades has documented consistent leaf and whole-plant
68 responses to elevated CO₂. At the leaf level, C₃ plants exhibit increased net photosynthesis rates
69 with reduced leaf nitrogen content, stomatal conductance, and photosynthetic capacity when
70 grown under elevated CO₂ compared to ambient conditions (Curtis, 1996; Drake *et al.*, 1997;
71 Nakano *et al.*, 1997; Medlyn *et al.*, 1999; Ainsworth *et al.*, 2002; Ainsworth & Long, 2005;
72 Bernacchi *et al.*, 2005; Ainsworth & Rogers, 2007; Crous *et al.*, 2010; Lee *et al.*, 2011; Pastore
73 *et al.*, 2019; Poorter *et al.*, 2022; Cui *et al.*, 2023). At the whole-plant level, CO₂ enrichment
74 increases total leaf area, which supports greater primary productivity and biomass accumulation
75 (Coleman *et al.*, 1993; Makino *et al.*, 1997; Ainsworth *et al.*, 2002; Ainsworth & Rogers, 2007;
76 Finzi *et al.*, 2007; Poorter *et al.*, 2022). Some studies suggest that elevated CO₂ may lead to
77 increased belowground carbon allocation and root:shoot ratios (Nie *et al.*, 2013; Stocker *et al.*, in
78 review), although these responses are inconsistently observed (Luo *et al.*, 1994; Poorter *et al.*,
79 2022).

80 Two hypotheses offer contrasting views on the role of nitrogen availability on plant
81 responses to elevated CO₂. The nitrogen limitation hypothesis posits that nitrogen availability
82 constrains plant responses to elevated CO₂, as nitrogen availability often limits net primary
83 productivity and influences the magnitude of the terrestrial carbon sink (Vitousek & Howarth,
84 1991; LeBauer & Treseder, 2008; Wieder *et al.*, 2015). Elevated CO₂ increases whole-plant
85 nitrogen demand to build new tissues, which may lead to greater nitrogen limitation of net
86 primary productivity without additional ecosystem nitrogen inputs (Luo *et al.*, 2004). Therefore,

87 the nitrogen limitation hypothesis predicts that increased nitrogen availability should enhance the
88 positive effects of elevated CO₂ on net primary productivity and biomass accumulation, provided
89 that nitrogen availability exceeds whole-plant demand for new tissues. Although some free-air
90 CO₂ enrichment experiments support this hypothesis (Reich *et al.*, 2006; Norby *et al.*, 2010),
91 these patterns are not consistently observed (Finzi *et al.*, 2006; Moore *et al.*, 2006; Liang *et al.*,
92 2016). Furthermore, the nitrogen limitation hypothesis implies that reduced leaf nitrogen content
93 and photosynthetic capacity under elevated CO₂ is the long-term result of progressive reductions
94 in ecosystem nitrogen availability. However, evidence shows that reductions in leaf nitrogen
95 content and photosynthetic capacity under elevated CO₂ are often decoupled from changes in
96 nitrogen availability (Crous *et al.*, 2010; Lee *et al.*, 2011; Pastore *et al.*, 2019), suggesting that
97 other factors might regulate these responses.

98 In contrast, the eco-evolutionary optimality hypothesis asserts that leaf-level
99 photosynthetic responses to elevated CO₂ are driven by the leaf-level demand to build and
100 maintain photosynthetic tissues and are independent of changes in nitrogen availability (Harrison
101 *et al.*, 2021). This hypothesis combines photosynthetic least-cost (Wright *et al.*, 2003; Prentice *et*
102 *al.*, 2014) and optimal coordination (Chen *et al.*, 1993; Maire *et al.*, 2012) theories, suggesting
103 that elevated CO₂ leads to a stronger downregulation in the maximum rate of Ribulose-1,5-
104 bisphosphate (RuBP) carboxylase/oxygenase (Rubisco) carboxylation (V_{cmax}) than the maximum
105 rate of electron transport for RuBP regeneration (J_{max}). The downregulation in V_{cmax} is attributed
106 to increased CO₂ substrate availability, which enhances Rubisco affinity for carboxylation
107 relative to oxygenation, thereby reducing the nitrogen demand to building and maintaining
108 additional Rubisco enzymes (Bazzaz, 1990). The eco-evolutionary optimality hypothesis posits
109 that plants should optimize leaf nitrogen allocation to photosynthetic capacity to efficiently use
110 available light while avoiding over-investment in Rubisco (Evans, 1989; Evans & Clarke, 2019).
111 This strategy enhances photosynthetic nitrogen-use efficiency and increases net photosynthesis
112 rates by increasing the co-limitation of Rubisco carboxylation and electron transport for RuBP
113 regeneration (Chen *et al.*, 1993; Maire *et al.*, 2012; Wang *et al.*, 2017; Smith *et al.*, 2019).
114 Previous studies support patterns predicted by the eco-evolutionary optimality hypothesis (Crous
115 *et al.*, 2010; Lee *et al.*, 2011; Smith & Keenan, 2020; Harrison *et al.*, 2021; Dong *et al.*, 2022;
116 Cui *et al.*, 2023), although these patterns have been rarely connected with concurrently measured
117 whole-plant responses.

118 The eco-evolutionary optimality hypothesis suggests that changes in leaf nitrogen
119 demand to build and maintain photosynthetic enzymes drive leaf-level photosynthetic responses
120 to elevated CO₂ independent of changes in nitrogen availability. However, the eco-evolutionary
121 optimality hypothesis does not discount the role of nitrogen availability on whole-plant responses
122 to elevated CO₂. The hypothesis suggests that the optimal whole-plant response to elevated CO₂
123 involves allocating surplus nitrogen not needed for photosynthetic enzyme maintenance toward
124 the construction of additional optimally coordinated leaves and other plant organs. Thus, the
125 extent to which plant responses to elevated CO₂ align with the nitrogen limitation or eco-
126 evolutionary optimality hypothesis may be a question of scale, with leaf-level responses being
127 influenced by leaf-level demand to build and maintain photosynthetic enzymes and whole-plant
128 responses being regulated by nitrogen availability.

129 Additionally, nitrogen acquisition strategies may impact how nitrogen availability affects
130 plant responses to elevated CO₂. Plants use different strategies for nitrogen acquisition, including
131 direct uptake pathways or symbioses with mycorrhizal fungi and symbiotic nitrogen-fixing
132 bacteria (Barber, 1962; Gutschick, 1981; Smith & Read, 2008). The carbon costs associated with
133 nitrogen acquisition vary among species with different dominant acquisition strategies and
134 depend on environmental factors such as atmospheric CO₂, temperature, light availability, and
135 nutrient availability (Fisher *et al.*, 2010; Brzostek *et al.*, 2014; Terrer *et al.*, 2018; Allen *et al.*,
136 2020; Perkowski *et al.*, 2021; Lu *et al.*, 2022; Peng *et al.*, 2023). These carbon costs of acquiring
137 nitrogen can influence nitrogen uptake and may scale up to influence nitrogen allocation to
138 different plant organs (Perkowski *et al.*, 2021; Waring *et al.*, 2023). Considering nitrogen
139 acquisition strategy is therefore important when examining plant responses to elevated CO₂
140 across nitrogen availability gradients. Few studies account for acquisition strategy when
141 considering the role of nitrogen availability on leaf and whole-plant responses to elevated CO₂
142 (Terrer *et al.*, 2018; Smith & Keenan, 2020). Despite this, some studies indicate that nitrogen
143 acquisition strategies with reduced carbon costs to acquire nitrogen may buffer the effect of
144 nitrogen limitation at the whole-plant level (Terrer *et al.*, 2018), but leaf-level responses remain
145 inconsistent (Terrer *et al.*, 2018; Smith & Keenan, 2020).

146 Here, we examined whether plant responses to elevated CO₂ aligned with the nitrogen
147 limitation or eco-evolutionary optimality hypothesis and assessed whether these patterns are
148 modified by nitrogen acquisition strategy. To do this, we conducted a growth chamber

149 experiment where *Glycine max* L. (Merr.) seedlings were grown under two CO₂ concentrations
150 (420, 1000 ppm CO₂), two inoculation treatments (with and without *Bradyrhizobium japonicum*),
151 and nine soil nitrogen fertilization treatments (0-630 ppm N) in a full-factorial design. We tested
152 the following hypotheses:

- 153 (1) According to the eco-evolutionary optimality hypothesis, elevated CO₂ will downregulate
154 V_{cmax} more than J_{max} , increasing the $J_{max}:V_{cmax}$ ratio and enhancing net photosynthesis
155 rates by approaching optimal coordination of Rubisco carboxylation and electron
156 transport for RuBP regeneration. Leaf photosynthetic responses to elevated CO₂ will be
157 independent of nitrogen fertilization and inoculation treatments, as these responses will
158 be driven by changes in leaf-level demand to build and maintain photosynthetic enzymes
159 and not by changes in nitrogen availability.
- 160 (2) Following the nitrogen limitation hypothesis, the positive effects of elevated CO₂ on total
161 leaf area and total biomass will be enhanced with increasing nitrogen fertilization. This
162 enhancement will be due to increased nitrogen uptake and reduced carbon costs to
163 acquire nitrogen with increasing nitrogen fertilization that will be stronger under elevated
164 CO₂. Biomass responses to elevated CO₂ will be driven by a greater increase in
165 belowground biomass than aboveground biomass, as plants will invest more in resource
166 acquisition strategies to meet any increased whole-plant nitrogen demand to build new
167 tissues.
- 168 (3) Inoculation with symbiotic nitrogen-fixing bacteria will not affect leaf photosynthetic
169 responses to elevated CO₂ but will enhance whole-plant responses. These responses will
170 be strongest under low nitrogen availability where inoculated plants will invest more in
171 nitrogen uptake through symbiotic nitrogen fixation; however, these patterns will
172 diminish with increasing nitrogen fertilization as plants acquire more nitrogen through
173 direct uptake pathways.

174

175 **Methods**

176 *Seed treatments and experimental design*

177 *Glycine max* L. (Merr) seeds (cultivar unknown, Territorial Seed Co., Cottage Grove, OR, USA)
178 were planted in 144 6-liter surface sterilized pots (NS-600, Nursery Supplies, Orange, CA, USA)
179 containing a steam-sterilized 70:30 volume: volume mix of *Sphagnum* peat moss (Premier

180 Horticulture, Quakertown, PA, USA) to sand (Pavestone, Atlanta, GA, USA). Before planting,
181 all *G. max* seeds were surface sterilized in 2% sodium hypochlorite for 3 minutes, followed by
182 three 3-minute washes with ultrapure water (MilliQ 7000; MilliporeSigma, Burlington, MA
183 USA). Subsets of surface-sterilized seeds were inoculated with *Bradyrhizobium japonicum*
184 (Verdesian N-Dure™ Soybean, Cary, NC, USA) in a slurry following manufacturer
185 recommendations (3.12 g inoculant and 241 g ultrapure water per 1 kg seed).

186 Seventy-two pots were randomly planted with surface-sterilized seeds inoculated with *B.*
187 *japonicum*, while the remaining 72 pots were planted with surface-sterilized uninoculated seeds.
188 Thirty-six pots in each inoculation treatment were placed in one of two atmospheric CO₂
189 treatments (420, 1000 µmol mol⁻¹ CO₂). CO₂ treatments were based on current ambient CO₂
190 concentrations and projections from the Intergovernmental Panel on Climate Change indicating
191 that CO₂ concentrations could surpass 1000 ppm by 2100 under the Shared Socioeconomic
192 Pathway 5-8.5 (IPCC, 2021). Plants in each unique inoculation-by-CO₂ treatment combination
193 received one of nine nitrogen fertilization treatments equivalent to 0 (0 mM), 35 (2.5 mM), 70 (5
194 mM), 105 (7.5 mM), 140 (10 mM), 210 (15 mM), 280 (20 mM), 350 (25 mM), or 630 ppm (45
195 mM) N. Nitrogen fertilization treatments were created using a modified Hoagland's solution
196 (Hoagland & Arnon, 1950) designed to keep concentrations of all other macronutrients and
197 micronutrients equivalent across treatments (Table S1). Plants received the same nitrogen
198 fertilization treatment twice per week in 150 mL doses as topical agents to the soil surface.
199 Plants were well-watered between fertilization treatments to ensure that physiology was not
200 limited by water availability.

201

202 *Growth chamber conditions*

203 Plants were randomly placed in one of six calibrated Percival LED-41L2 growth chambers
204 (Percival Scientific Inc., Perry, IA, USA) over two experimental iterations due to chamber space
205 limitation. The first iteration included all plants grown under elevated CO₂, while the second
206 included all plants grown under ambient CO₂. Average (\pm SD) CO₂ concentrations across
207 chambers throughout the experiment were 439 ± 5 µmol mol⁻¹ CO₂ for the ambient treatment and
208 989 ± 4 µmol mol⁻¹ CO₂ for the elevated treatment.

209 Daytime growth conditions were simulated using a 16-hour photoperiod, with incoming
210 light radiation set to chamber maximum (mean \pm SD: 1230 ± 12 µmol m⁻² s⁻¹ across chambers), air

temperature set to 25°C, and relative humidity set to 50%. The remaining 8-hour period simulated nighttime growing conditions, with incoming light radiation set to 0 $\mu\text{mol m}^{-2} \text{s}^{-1}$, chamber temperature set to 17°C, and relative humidity set to 50%. Transitions between daytime and nighttime growing conditions were simulated by ramping incoming light radiation in 45-minute increments and temperature in 90-minute increments over 3 hours (Table S2).

Plants grew under average (\pm SD) daytime light intensity of $1049 \pm 27 \mu\text{mol m}^{-2} \text{s}^{-1}$, including ramping periods. In the elevated CO₂ iteration, plants grew under $24.0 \pm 0.2^\circ\text{C}$ during the day, $16.4 \pm 0.8^\circ\text{C}$ during the night, and $51.6 \pm 0.4\%$ relative humidity. In the ambient CO₂ iteration, plants grew under $23.9 \pm 0.2^\circ\text{C}$ during the day, $16.0 \pm 1.4^\circ\text{C}$ during the night, and $50.3 \pm 0.2\%$ relative humidity. Any differences in climate conditions across the six chambers were accounted for by shuffling the same group of plants throughout the growth chambers. This process was done by iteratively moving the group of plants on the top rack of a chamber to the bottom rack of the same chamber while simultaneously moving the group of plants on the bottom rack of a chamber to the top rack of the adjacent chamber. Plants were moved within and across chambers daily during each experiment iteration.

226

227 *Leaf gas exchange measurements*

Leaf gas exchange measurements were collected in all plants on the seventh week of development, before the onset of reproduction. All gas exchange measurements were collected on the center leaflet of the most recent fully expanded trifoliate leaflet set using LI-6800 portable photosynthesis machines configured with a 6800-01A fluorometer head and 6 cm² aperture (LI-COR Biosciences, Lincoln, NE, USA). Specifically, net photosynthesis rates (A_{net} ; $\mu\text{mol m}^{-2} \text{s}^{-1}$), stomatal conductance rates (g_{sw} ; $\text{mol m}^{-2} \text{s}^{-1}$), and intercellular CO₂ concentrations (C_i ; $\mu\text{mol mol}^{-1}$) were measured across a range of atmospheric CO₂ concentrations (i.e., an A_{net}/C_i curve) using the Dynamic Assimilation™ Technique. The Dynamic Assimilation™ Technique corresponds well with traditional steady-state A_{net}/C_i curves (Saathoff & Welles, 2021; Tejera-Nieves *et al.*, 2024). A_{net}/C_i curves were generated along a reference CO₂ ramp down from 420 $\mu\text{mol mol}^{-1}$ CO₂ to 20 $\mu\text{mol mol}^{-1}$ CO₂, followed by a ramp up from 20 $\mu\text{mol mol}^{-1}$ CO₂ to 1620 $\mu\text{mol mol}^{-1}$ CO₂ after a 90-second wait period at 20 $\mu\text{mol mol}^{-1}$ CO₂. The ramp rate for each curve was set to 200 $\mu\text{mol mol}^{-1} \text{ min}^{-1}$, logging every five seconds, generating 96 data points per response curve. All A_{net}/C_i curves were conducted after A_{net} and g_{sw} stabilized in a LI-6800 cuvette set to a

242 500 mol s⁻¹ flow rate, 10000 rpm mixing fan speed, 1.5 kPa vapor pressure deficit, 25°C leaf
243 temperature, 2000 $\mu\text{mol m}^{-2} \text{s}^{-1}$ incoming light radiation, and initial reference CO₂ concentration
244 set to 420 $\mu\text{mol mol}^{-1}$.

245 Snapshot A_{net} measurements were extracted from each A_{net}/C_i curve, both at a common
246 CO₂ concentration, 420 $\mu\text{mol mol}^{-1}$ CO₂ ($A_{\text{net},420}$; $\mu\text{mol m}^{-2} \text{s}^{-1}$), and growth CO₂ concentration,
247 420 and 1000 $\mu\text{mol mol}^{-1}$ CO₂ ($A_{\text{net},\text{gc}}$; $\mu\text{mol m}^{-2} \text{s}^{-1}$). We quantified $A_{\text{net},420}$ to gauge relative
248 investment in photosynthetic tissues between treatment combinations and $A_{\text{net},\text{gc}}$ to quantify
249 photosynthetic performance between treatment combinations. Dark respiration (R_d ; $\mu\text{mol m}^{-2} \text{s}^{-1}$)
250 measurements were collected on the same leaflet used to generate A_{net}/C_i curves following at
251 least a 30-minute period of darkness. Dark respiration measurements were collected on a 5-
252 second log interval for 60 seconds after the leaf stabilized in a LI-6800 cuvette set to a 500 mol s⁻¹
253 flow rate, 10000 rpm mixing fan speed, 1.5 kPa vapor pressure deficit, 25°C leaf temperature,
254 and 420 $\mu\text{mol mol}^{-1}$ reference CO₂ concentration (regardless of CO₂ treatment), with incoming
255 light radiation set to 0 $\mu\text{mol m}^{-2} \text{s}^{-1}$. A single dark respiration value was determined for each
256 leaflet by calculating the mean dark respiration value across the logging interval.

257

258 *A/C_i curve-fitting and parameter estimation*

259 A_{net}/C_i curves were fit using the ‘fitaci’ function in the ‘plantecophys’ R package (Duursma,
260 2015). This function estimates the apparent maximum rate of Rubisco carboxylation (V_{cmax} ;
261 $\mu\text{mol m}^{-2} \text{s}^{-1}$) and apparent maximum rate of electron transport for RuBP regeneration (J_{max} ;
262 $\mu\text{mol m}^{-2} \text{s}^{-1}$) based the Farquhar et al. (1980) biochemical model of C₃ photosynthesis. Triose
263 phosphate utilization (TPU) limitation was included as an additional rate-limiting step after
264 visually observing clear TPU limitation for most curves. All curve fits included measured dark
265 respiration values. As A_{net}/C_i curves were generated using a common leaf temperature (25°C),
266 curves were fit using Michaelis-Menten coefficients for Rubisco affinity to CO₂ (K_c ; $\mu\text{mol mol}^{-1}$)
267 and O₂ (K_o ; mmol mol⁻¹), and the CO₂ compensation point (I^* ; $\mu\text{mol mol}^{-1}$) reported in
268 Bernacchi et al. (2001). Specifically, K_c was set to 404.9 $\mu\text{mol mol}^{-1}$, K_o was set to 278.4 μmol
269 mol⁻¹, and I^* was set to 42.75 $\mu\text{mol mol}^{-1}$. V_{cmax} , J_{max} , and R_d estimates are referenced throughout
270 the rest of the paper as $V_{\text{cmax}25}$, $J_{\text{max}25}$, and R_{d25} .

271

272 *Leaf trait measurements*

273 The leaflet used for A_{net}/C_i curves and dark respiration measurements was harvested immediately
274 following gas exchange measurements. Images of each focal leaflet were curated using a flat-bed
275 scanner to determine fresh leaf area using the 'LeafArea' R package (Katabuchi, 2015), which
276 automates leaf area calculations using ImageJ software (Schneider *et al.*, 2012). Post-processed
277 images were visually assessed to check against errors in the automation process. Each focal
278 leaflet was dried at 65°C for at least 48 hours, weighed, and ground until homogenized. Leaf
279 mass per area (M_{area} ; g m⁻²) was calculated as the ratio of dry leaflet biomass to fresh leaflet area.
280 Leaf nitrogen content (N_{mass} ; gN g⁻¹) was quantified using a subsample of ground and
281 homogenized leaflet tissue through elemental combustion (Costech-4010, Costech, Inc.,
282 Valencia, CA, USA). Leaf nitrogen content per unit leaf area (N_{area} ; gN m⁻²) was calculated by
283 multiplying N_{mass} and M_{area} . Photosynthetic nitrogen-use efficiency ($PNUE_{\text{gc}}$; μmol CO₂ g⁻¹ N s⁻¹)
284 was estimated as the ratio of $A_{\text{net,gc}}$ to N_{area} .

285 Chlorophyll content was extracted from a second leaflet in the same trifoliate leaf set as
286 the leaf used to generate A_{net}/C_i curves. A cork borer was used to punch 3-5 0.6 cm² disks from
287 the leaflet. Images of each set of leaflet disks were curated using a flat-bed scanner to determine
288 wet leaf area, again quantified using the 'LeafArea' R package (Katabuchi, 2015). Leaflet disks
289 were shuttled into a test tube containing 10 mL dimethyl sulfoxide, vortexed, and incubated at
290 65°C for 120 minutes (Barnes *et al.*, 1992). Incubated test tubes were vortexed again before
291 being loaded in 150 μL triplicate aliquots to a 96-well plate. Dimethyl sulfoxide was loaded in
292 each plate as a single 150 μL triplicate aliquot and used as a blank. Absorbance measurements at
293 649 nm (A_{649}) and 665 nm (A_{665}) were recorded using a plate reader (Biotek Synergy H1; Biotek
294 Instruments, Winooski, VT USA), with triplicate measurements averaged and corrected by the
295 mean of the blank absorbance value. Blank-corrected absorbance values were used to estimate
296 chlorophyll *a* (Chl_a ; μg mL⁻¹) and chlorophyll *b* (Chl_b ; μg mL⁻¹) following equations from
297 Wellburn (1994):

298 $Chl_a = 12.19A_{665} - 3.45A_{649}$ (1)

299 and

300 $Chl_b = 21.99A_{649} - 5.32A_{665}$ (2)

301 Chl_a and Chl_b were converted to mmol mL⁻¹ using the molar masses of chlorophyll *a* (893.51 g
302 mol⁻¹) and chlorophyll *b* (907.47 g mol⁻¹), then added together to calculate the total chlorophyll
303 content in dimethyl sulfoxide extractant (mmol mL⁻¹). Total chlorophyll content (mmol) was

304 determined by multiplying the total chlorophyll content in dimethyl sulfoxide by the volume of
305 dimethyl sulfoxide extractant (10 mL). Area-based chlorophyll content (Chl_{area} ; mmol m⁻²) was
306 then calculated by dividing the total chlorophyll content by the total area of the leaflet disks.

307

308 *Whole-plant measurements*

309 All individuals were harvested, and biomass of major organ types (leaves, stems, roots, and
310 nodules when present) were separated immediately following gas exchange measurements. Fresh
311 leaf area of all harvested leaflets was measured using a LI-3100C (LI-COR Biosciences, Lincoln,
312 Nebraska, USA). Total fresh leaf area (cm²) was calculated as the sum of all leaflet areas,
313 including those used for gas exchange and chlorophyll extractions. Harvested material was
314 separately dried in an oven set to 65°C for at least 48 hours to a constant mass, weighed, and
315 then was ground to homogeneity. Leaves and root nodules were ground using a mortar and
316 pestle, while stems and roots were ground using an E3300 Single Speed Mini Cutting Mill
317 (Eberbach Corp., MI, USA). Total biomass (g) was calculated as the sum of dry leaf, stem, root,
318 and root nodule biomass. Carbon and nitrogen content was measured for each organ type through
319 elemental combustion (Costech-4010, Costech, Inc., Valencia, CA, USA) using ground and
320 homogenized organ tissue subsamples. The ratio of root nodule biomass to root biomass was
321 calculated as an indicator of plant investment toward nitrogen fixation relative to other uptake
322 pathways (e.g., direct uptake). The root:shoot ratio (unitless) was calculated as the ratio of
323 belowground biomass (root and root nodule biomass) to shoot biomass (leaf and stem biomass).
324 Leaf, stem, and root mass fractions were calculated as the dry biomass of each respective organ
325 per unit total biomass (g g⁻¹ in all cases).

326 Belowground biomass carbon costs to acquire nitrogen were quantified as the ratio of
327 belowground biomass carbon to whole-plant nitrogen biomass (g C g N⁻¹) (Perkowski *et al.*,
328 2021). Belowground biomass carbon (g C) was calculated as the sum of root and root nodule
329 carbon biomass. Root carbon biomass and root nodule carbon biomass were calculated as the
330 product of the organ biomass and respective organ carbon content. Whole-plant nitrogen biomass
331 (g N) was calculated as the sum of total leaf, stem, root, and root nodule nitrogen biomass. Leaf,
332 stem, root, and root nodule nitrogen biomass was calculated as the product of the organ biomass
333 and respective organ nitrogen content. This calculation does not account for additional carbon

334 costs associated with respiration, root exudation, or root turnover and may underestimate carbon
335 costs to acquire nitrogen (Perkowski *et al.*, 2021).

336

337 *Statistical analyses*

338 Uninoculated plants with substantial root nodule formation (root nodule biomass: root biomass
339 values greater than 0.05 g g⁻¹) were removed from analyses following the assumption that plants
340 were incompletely sterilized or contaminated. This decision resulted in the removal of sixteen
341 plants from the analysis: two plants in the elevated CO₂ treatment that received 35 ppm N, three
342 plants in the elevated CO₂ treatment that received 70 ppm N, one plant in the elevated CO₂
343 treatment that received 210 ppm N, two plants in the elevated CO₂ treatment that received 280
344 ppm N, two plants in the ambient CO₂ treatment that received 0 ppm N, three plants in the
345 ambient CO₂ treatment that received 70 ppm N, two plants in the ambient CO₂ treatment that
346 received 105 ppm N, and one plant in the ambient CO₂ treatment that received 280 ppm N.

347 A series of linear mixed-effects models were built to investigate the impacts of CO₂
348 concentration, nitrogen fertilization, and inoculation on *G. max* leaf nitrogen content, leaf gas
349 exchange, total leaf area, biomass and biomass allocation, and plant investment in symbiotic
350 nitrogen fixation. All models included CO₂ treatment as a categorical fixed effect, inoculation
351 treatment as a categorical fixed effect, and nitrogen fertilization as a continuous fixed effect, with
352 all possible interaction terms between all three fixed effects included. Models accounted for
353 climatic differences between chambers across experiment iterations by including a random
354 intercept term that nested the starting chamber rack within CO₂ treatment. Models with this
355 independent variable structure were created for each of the following dependent variables: N_{area} ,
356 M_{area} , N_{mass} , Chl_{area} , $A_{\text{net},420}$, $A_{\text{net,gc}}$, $V_{\text{cmax}25}$, $J_{\text{max}25}$, $J_{\text{max}25}:V_{\text{cmax}25}$, $R_{\text{d}25}$, $PNUE_{\text{gc}}$, total leaf area,
357 total biomass, total leaf biomass, stem biomass, root biomass, root nodule biomass, root:shoot
358 ratio, leaf mass fraction, stem mass fraction, root mass fraction, belowground biomass carbon
359 costs to acquire nitrogen, belowground biomass carbon, whole-plant nitrogen biomass, and the
360 root nodule biomass:root biomass ratio.

361 Shapiro-Wilk tests of normality were used to assess whether linear mixed-effects models
362 satisfied residual normality assumptions. Models for N_{area} , N_{mass} , Chl_{area} , $A_{\text{net},420}$, $A_{\text{net,gc}}$, $V_{\text{cmax}25}$,
363 $J_{\text{max}25}$, $J_{\text{max}25}:V_{\text{cmax}25}$, $R_{\text{d}25}$, $PNUE_{\text{gc}}$, total leaf area, leaf mass fraction, stem mass fraction,
364 belowground biomass carbon, and whole-plant nitrogen biomass satisfied residual normality

365 assumptions without data transformation. Models for M_{area} , root:shoot ratio, belowground
366 biomass carbon costs to acquire nitrogen, and root mass fraction satisfied residual normality
367 assumptions with a natural log data transformation. Models for total biomass, leaf biomass, stem
368 biomass, root biomass, root nodule biomass, and root nodule biomass: root biomass satisfied
369 residual normality assumptions with a square root data transformation.

370 In all models, the ‘lmer’ function in the ‘lme4’ R package (Bates *et al.*, 2015) was used to
371 fit each model, and the ‘Anova’ function in the ‘car’ R package (Fox & Weisberg, 2019) was
372 used to calculate Type II Wald's χ^2 and determine the significance ($\alpha=0.05$) of each fixed effect
373 coefficient. The ‘emmeans’ R package (Lenth, 2019) was used to conduct post-hoc comparisons
374 using Tukey's tests, where degrees of freedom were approximated using the Kenward-Roger
375 approach (Kenward & Roger, 1997). Trendlines and error ribbons representing the 95%
376 confidence intervals were drawn in all figures using ‘emmeans’ outputs across the range in
377 nitrogen fertilization values. All analyses and plots were conducted in R version 4.1.0 (R Core
378 Team, 2021). Results for N_{mass} and M_{area} and organ biomasses are summarized in the
379 *Supplemental Material* (Table S3, S5, Fig. S1).

380

381 **Results**

382 *Leaf nitrogen content*

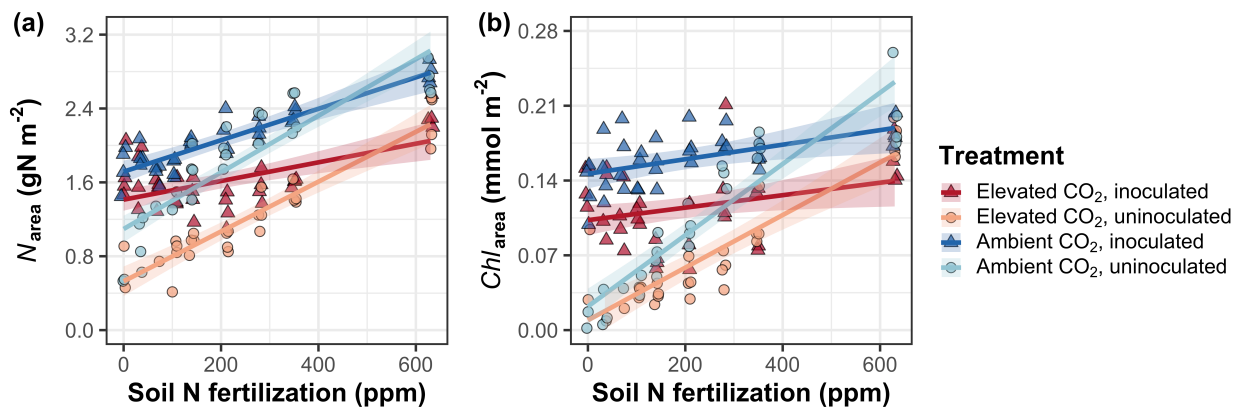
383 Elevated CO₂ reduced N_{area} and Chl_{area} by 29% and 30%, respectively ($p<0.001$ in both cases;
384 Table 1; Fig. 1). Increasing nitrogen fertilization increased N_{area} ($p<0.001$; Table 1; Fig. 1) more
385 strongly under ambient CO₂ than elevated CO₂ (CO₂-by-nitrogen fertilization interaction:
386 $p<0.05$; Table 1), resulting in a stronger reduction in N_{area} under elevated CO₂ with increasing
387 nitrogen fertilization than ambient CO₂ (Fig. S2). Uninoculated plants experienced a stronger
388 reduction in N_{area} under elevated CO₂ than inoculated plants (CO₂-by-inoculation interaction:
389 $p<0.05$; Table 1). Increasing nitrogen fertilization increased N_{area} and Chl_{area} ($p<0.001$ in both
390 cases; Table 1; Fig. 1) more strongly in uninoculated plants than inoculated plants (inoculation-
391 by-nitrogen fertilization interaction: $p<0.001$ in both cases; Table 1).

392 **Table 1** Effects of CO₂ concentration, inoculation, and nitrogen fertilization on area-based leaf
 393 nitrogen content and chlorophyll content*

		<i>N_{area}</i>		<i>Chl_{area}</i>	
	df	χ^2	<i>p</i>	χ^2	<i>p</i>
CO ₂	1	155.908	<0.001	62.056	<0.001
Inoculation (I)	1	86.029	<0.001	133.828	<0.001
N fertilization (N)	1	316.408	<0.001	156.659	<0.001
CO ₂ × I	1	4.729	0.030	1.647	0.199
CO ₂ × N	1	5.723	0.017	2.780	0.095
I × N	1	43.381	<0.001	73.494	<0.001
CO ₂ × I × N	1	0.489	0.484	2.123	0.145

394 *Significance determined using Type II Wald χ^2 tests ($\alpha=0.05$). *P*-values less than 0.05 are in
 395 bold. Key: df=degrees of freedom, χ^2 =Wald chi-square test statistic, *N_{area}*=leaf nitrogen content
 396 per unit leaf area (gN m⁻²), *Chl_{area}*=chlorophyll content per unit leaf area (mmol m⁻²)

397

398 **Figure 1**

399
400 **Figure 1** Effects of CO_2 concentration, inoculation, and nitrogen fertilization on leaf nitrogen per
401 unit leaf area (a) and chlorophyll content per unit leaf area (b). Nitrogen fertilization is on the x-
402 axis in both panels. Red shaded points and trendlines indicate plants grown under elevated CO_2 ,
403 while blue shaded points and trendlines indicate plants grown under ambient CO_2 . Light blue and
404 light red circular points and trendlines indicate measurements collected from uninoculated plants,
405 while dark blue and dark red triangular points indicate measurements collected from inoculated
406 plants. Solid trendlines indicate regression slopes that are different from zero ($p < 0.05$), while
407 dashed trendlines indicate slopes that are not distinguishable from zero ($p > 0.05$). Error ribbons
408 of each trendline represent the upper and lower 95% confidence intervals.
409

410 *Gas exchange*
411 Elevated CO₂ decreased $A_{\text{net},420}$ by 17% and increased $A_{\text{net,gc}}$ by 33% ($p<0.001$ in both cases;
412 Table 2). Increasing nitrogen fertilization increased $A_{\text{net},420}$ and $A_{\text{net,gc}}$ similarly between CO₂
413 treatments (CO₂-by-nitrogen fertilization interaction: $p>0.05$; Table 2; Fig. 2a). Inoculated plants
414 experienced a stronger increase in $A_{\text{net,gc}}$ under elevated CO₂ than uninoculated plants (CO₂-by-
415 inoculation interaction: $p<0.05$; Table 2). Increasing nitrogen fertilization increased $A_{\text{net},420}$ and
416 $A_{\text{net,gc}}$ ($p<0.001$ in both cases; Table 2) more strongly in uninoculated plants than inoculated
417 plants (inoculation-by-nitrogen fertilization interaction: $p<0.001$ in both cases; Fig. 2a-b).

418 Elevated CO₂ decreased $V_{\text{cmax}25}$ by 16% and $J_{\text{max}25}$ by 10%, which increased $J_{\text{max}25}:V_{\text{cmax}25}$
419 by 8% ($p<0.05$ in all cases; Table 2). Increasing nitrogen fertilization increased $V_{\text{cmax}25}$ and
420 $J_{\text{max}25}$, but decreased $J_{\text{max}25}:V_{\text{cmax}25}$, similarly between CO₂ (CO₂-by-nitrogen fertilization
421 interaction: $p>0.05$ in all cases; Table 2; Fig. 2b-d) and inoculation treatments (CO₂-by-
422 inoculation interaction: $p>0.05$ in all cases; Table 2). Increasing nitrogen fertilization increased
423 $V_{\text{cmax}25}$ and $J_{\text{max}25}$ and decreased $J_{\text{max}25}:V_{\text{cmax}25}$ ($p<0.001$; Table 2), but this pattern was only
424 observed in uninoculated plants (inoculation-by-nitrogen fertilization interaction: $p<0.05$ in all
425 cases).

426 CO₂ treatment had no effect on $R_{\text{d}25}$ ($p>0.05$; Table S4). Increasing nitrogen fertilization
427 increased $R_{\text{d}25}$ ($p<0.05$; Table S4), but this pattern was only observed in uninoculated plants
428 (inoculation-by-nitrogen fertilization interaction: $p<0.001$; Table S4; Fig. S3a). Inoculated plants
429 exhibited marginally greater $R_{\text{d}25}$ than uninoculated plants ($p<0.1$; Table S4)

430

431 *Photosynthetic nitrogen-use efficiency*

432 Elevated CO₂ increased $PNUE_{\text{gc}}$ by 97% ($p<0.001$; Table S4; Fig. S3b) due to a 33% increase in
433 $A_{\text{net,gc}}$ (Fig. 2a) and 29% decrease in N_{area} (Fig. 1a). Increasing nitrogen fertilization decreased
434 $PNUE_{\text{gc}}$ ($p<0.001$; Table S4) more strongly under elevated CO₂ (CO₂-by-nitrogen fertilization
435 interaction: $p<0.05$; Table S4; Fig. S3b), leading to a weaker increase in $PNUE_{\text{gc}}$ due to elevated
436 CO₂ with increasing nitrogen fertilization (Fig. S4). Increasing nitrogen fertilization decreased
437 $PNUE_{\text{gc}}$ ($p<0.001$; Table S4), but this pattern was only observed in inoculated plants
438 (inoculation-by-nitrogen fertilization interaction: $p<0.05$; Table S4; Fig. S3b).

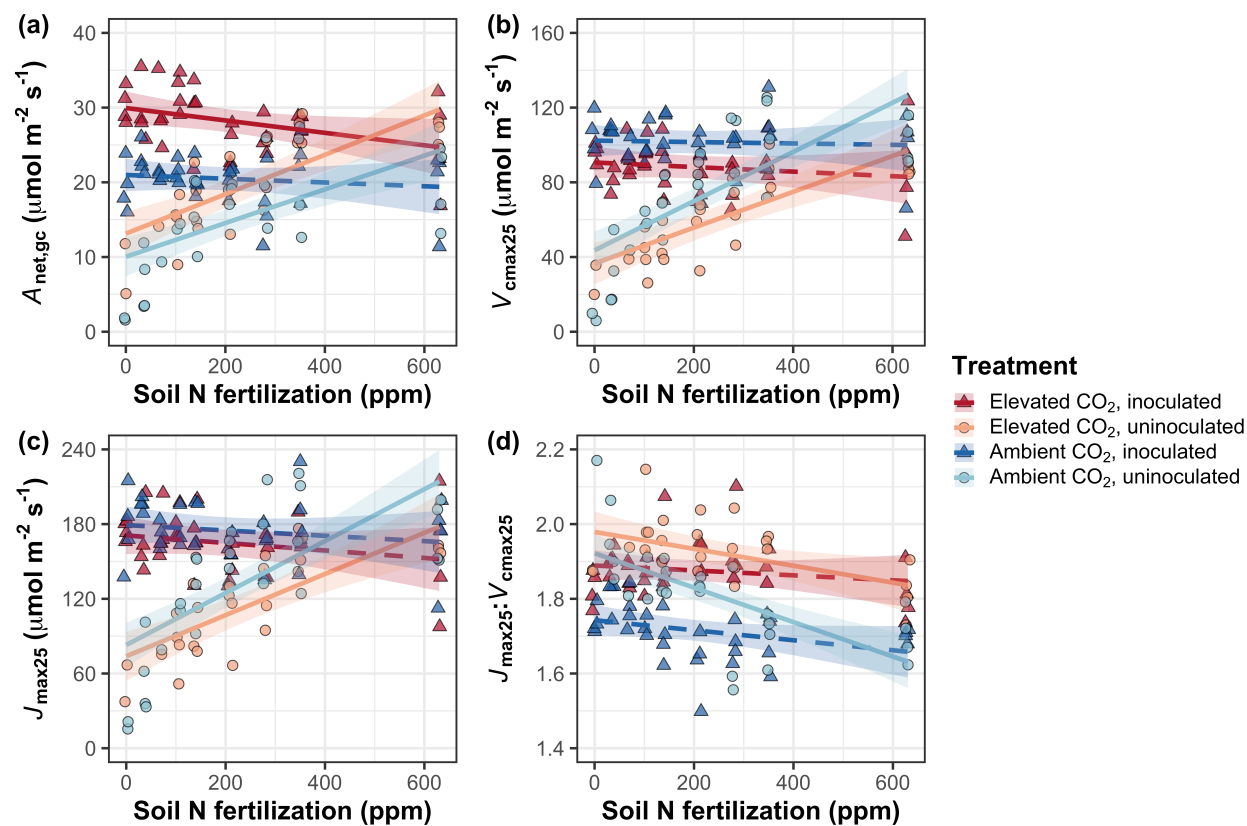
439

440 **Table 2** Effects of CO₂ concentration, inoculation, and nitrogen fertilization on leaf gas exchange*

	<i>A</i> _{net,420}			<i>A</i> _{net,gc}			<i>V</i> _{cmax25}			<i>J</i> _{max25}		<i>J</i> _{max25:} <i>V</i> _{cmax25}	
	df	χ^2	p	χ^2	p	χ^2	p	χ^2	p	χ^2	p	χ^2	p
CO ₂	1	15.747	<0.001	52.716	<0.001	18.039	<0.001	6.042	0.014	92.010	<0.001		
Inoculation (I)	1	77.137	<0.001	83.008	<0.001	98.579	<0.001	85.064	<0.001	27.768	<0.001		
N fertilization (N)	1	11.986	<0.001	14.658	<0.001	37.053	<0.001	25.356	<0.001	28.147	<0.001		
CO ₂ × I	1	1.032	0.310	5.634	0.018	0.065	0.799	0.667	0.414	2.916	0.088		
CO ₂ × N	1	1.998	0.158	0.135	0.713	1.758	0.185	0.742	0.389	3.210	0.073		
I × N	1	46.800	<0.001	50.774	<0.001	60.394	<0.001	57.41	<0.001	9.607	0.002		
CO ₂ × I × N	1	0.002	0.964	1.332	0.248	0.748	0.387	0.377	0.539	1.102	0.294		

441 *Significance determined using Type II Wald χ^2 tests ($\alpha=0.05$). P-values less than 0.05 are in bold. Key: df=degrees of freedom,442 χ^2 =Wald chi-square test statistic, $A_{\text{net},420}$ =net photosynthesis rate at 420 $\mu\text{mol mol}^{-1}$ CO₂ ($\mu\text{mol m}^{-2} \text{s}^{-1}$), $A_{\text{net,gc}}$ =net photosynthesis rate443 at under growth CO₂ condition ($\mu\text{mol m}^{-2} \text{s}^{-1}$), V_{cmax25} =maximum rate of Rubisco carboxylation at 25°C ($\mu\text{mol m}^{-2} \text{s}^{-1}$),444 J_{max25} =maximum rate of electron transport for RuBP regeneration at 25°C ($\mu\text{mol m}^{-2} \text{s}^{-1}$), $J_{\text{max25}}:V_{\text{cmax25}}$ =ratio of J_{max25} to V_{cmax25}

445 (unitless)

446 **Figure 2**

447

448 **Figure 2** Effects of CO₂, inoculation, and nitrogen fertilization on net photosynthesis measured
 449 under growth CO₂ concentration (a), the maximum rate of Rubisco carboxylation at 25°C (b), the
 450 maximum rate of electron transport for RuBP regeneration at 25°C (c), and the ratio of the
 451 maximum rate of electron transport for RuBP regeneration to the maximum rate of Rubisco
 452 carboxylation (d). Nitrogen fertilization is on the x-axis in all panels. Red shaded points and
 453 trendlines indicate plants grown under elevated CO₂, while blue shaded points and trendlines
 454 indicate plants grown under ambient CO₂. Light blue and light red circular points and trendlines
 455 indicate measurements collected from uninoculated plants, while dark blue and dark red
 456 triangular points indicate measurements collected from inoculated plants. Solid trendlines
 457 indicate regression slopes that are different from zero ($p < 0.05$), while dashed trendlines indicate
 458 slopes that are not distinguishable from zero ($p > 0.05$). Error ribbons of each trendline represent
 459 the upper and lower 95% confidence intervals.

460 *Total leaf area and total biomass*
461 Elevated CO₂ increased total leaf area and total biomass by 51% and 102%, respectively
462 ($p<0.001$ in both cases; Table 3). Increasing nitrogen fertilization increased total leaf area and
463 total biomass ($p<0.001$ in both cases; Table 3) more strongly under elevated CO₂ than ambient
464 CO₂ (CO₂-by-nitrogen fertilization interaction: $p<0.001$ in both cases; Table 3), leading to an
465 amplified positive effect of elevated CO₂ on total leaf area and total biomass with increasing
466 nitrogen fertilization (Fig. 3). Increasing nitrogen fertilization increased total leaf area and total
467 biomass ($p<0.001$ in both cases; Table 3) more strongly in uninoculated plants than inoculated
468 plants (inoculation-by-nitrogen fertilization interaction: $p<0.001$; Table 3; Fig. 3).

469

470 *Biomass partitioning*

471 The root:shoot ratio decreased under elevated CO₂ ($p<0.05$; Table 3; Fig. 3c), although this
472 pattern was only observed in inoculated plants (CO₂-by-inoculation interaction: $p<0.05$; Table 3,
473 Fig. 3c). Reductions in the root:shoot ratio under elevated CO₂ were driven by an increase in the
474 leaf mass fraction under elevated CO₂ ($p<0.001$; Table S5) that was only observed in inoculated
475 plants (CO₂-by-inoculation interaction: $p<0.05$; Table S5). CO₂ treatment had no effect on stem
476 mass fraction ($p>0.05$; Table S5), although an interaction between CO₂ and inoculation treatment
477 indicated that elevated CO₂ increased the root mass fraction in inoculated plants (CO₂-by-
478 inoculation interaction: $p<0.05$; Table S5). Increasing nitrogen fertilization decreased the
479 root:shoot ratio ($p<0.001$; Table 3), a pattern that was marginally stronger in uninoculated plants
480 than inoculated plants (CO₂-by-inoculation interaction: $p=0.051$; Table 3; Fig. 3c). Increasing
481 nitrogen fertilization increased the leaf mass fraction and decreased the root mass fraction
482 ($p<0.001$ in both cases; Table S5), but these patterns only occurred in uninoculated plants
483 (inoculation-by-nitrogen fertilization interaction: $p<0.05$ in both cases; Table S5). Increasing
484 nitrogen fertilization increased stem mass fraction ($p<0.001$; Table S5), but these patterns only
485 occurred in inoculated plants (inoculation-by-nitrogen fertilization interaction: $p<0.001$; Table
486 S5).

487

488 *Belowground biomass carbon cost to acquire nitrogen*

489 Elevated CO₂ increased belowground biomass carbon costs to acquire nitrogen ($p<0.001$; Table
490 3) more strongly in uninoculated plants than inoculated plants (CO₂-by-inoculation interaction:

491 $p<0.001$; Table 3). Increasing nitrogen fertilization decreased carbon costs to acquire nitrogen
492 ($p<0.001$; Table 3) more strongly in uninoculated plants than inoculated plants (inoculation-by-
493 nitrogen fertilization: $p<0.001$; Table 3; Fig. 3d). Interactions between inoculation and nitrogen
494 fertilization treatments were more pronounced when plants were grown under elevated CO₂
495 (CO₂-by-inoculation-by-nitrogen fertilization interaction: $p<0.05$; Fig. 3d). This pattern was
496 driven by a strong negative effect of increasing nitrogen fertilization on carbon costs to acquire
497 nitrogen in uninoculated plants grown under elevated CO₂ (Tukey: $p<0.001$) coupled with no
498 nitrogen fertilization effect in inoculated plants grown under elevated CO₂ (Tukey: $p<0.001$).
499 Under ambient CO₂, increasing nitrogen fertilization decreased carbon costs to acquire nitrogen
500 similarly between inoculation treatments (Tukey: $p>0.05$).

501 Elevated CO₂ increased belowground biomass carbon by 93% and increased whole-plant
502 nitrogen biomass by 26% ($p<0.001$ in both cases; Table S6). Increasing nitrogen fertilization
503 increased belowground biomass carbon and whole-plant nitrogen biomass more strongly under
504 elevated CO₂ than ambient CO₂ (CO₂-by-nitrogen fertilization interaction: $p<0.001$; Table S6;
505 Fig. S5). These patterns resulted in an amplified positive effect of elevated CO₂ on belowground
506 biomass carbon and whole-plant nitrogen biomass with increasing nitrogen fertilization, though
507 this pattern was stronger for whole-plant nitrogen biomass than belowground biomass carbon
508 (Fig. S5). Increasing nitrogen fertilization increased belowground biomass carbon and whole-
509 plant nitrogen biomass ($p<0.001$; Table S6) more strongly in uninoculated plants than inoculated
510 plants (inoculation-by-nitrogen fertilization interaction: $p<0.001$ in both cases; Table S6; Fig.
511 S5).

512

513 *Plant investment toward symbiotic nitrogen fixation*

514 CO₂ treatment had no effect on root nodule: root biomass ($p>0.05$; Table 3; Fig. 4) despite
515 stronger positive effects of elevated CO₂ on root biomass (96% increase; $p<0.001$; Table S5)
516 than root nodule biomass (70% increase; $p<0.001$; Table S5). Increasing nitrogen fertilization
517 decreased root nodule: root biomass ($p<0.001$; Table 3) more strongly in inoculated plants than
518 uninoculated plants (inoculation-by-nitrogen fertilization interaction: $p<0.001$; Table 3; Fig. 4).

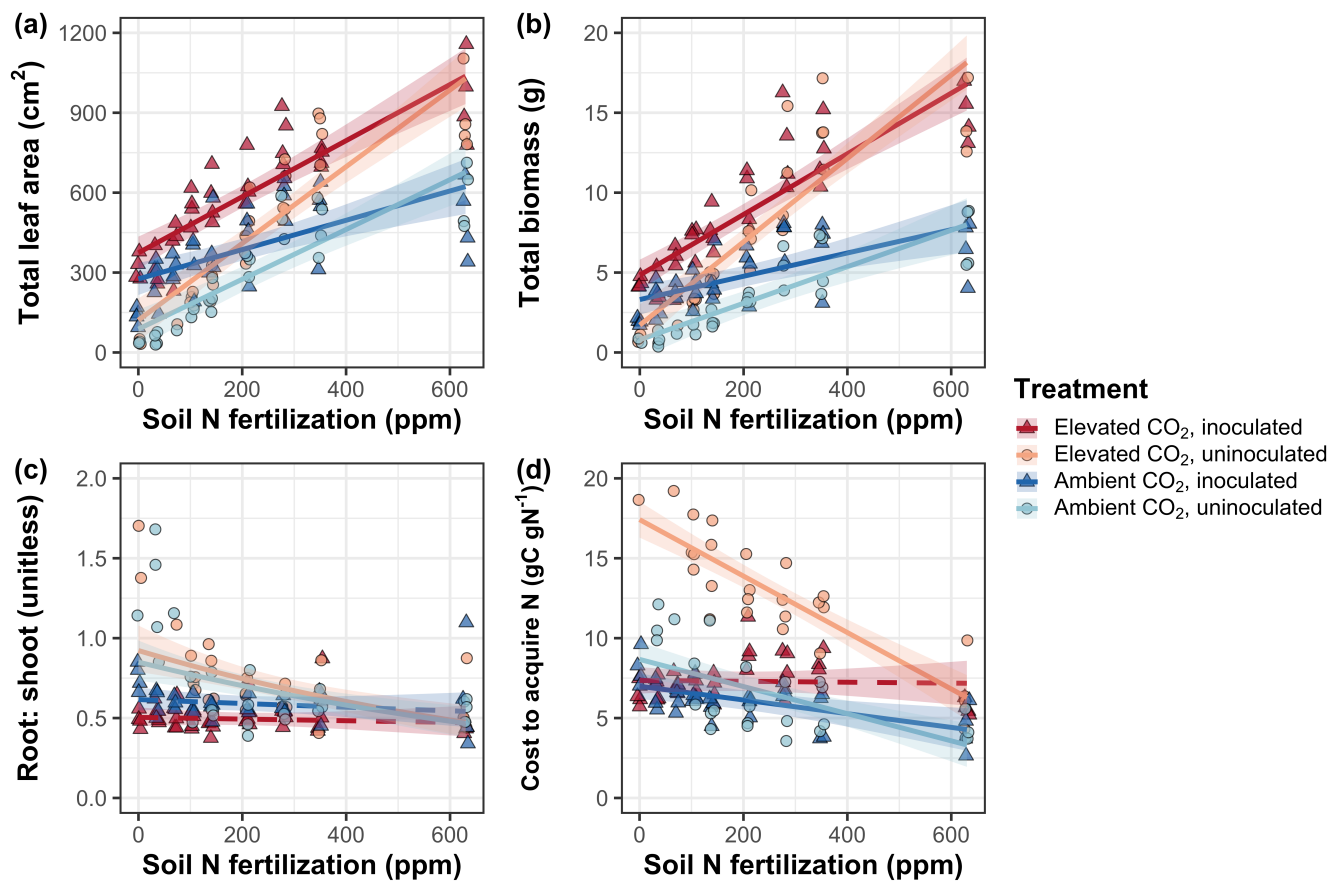
519

520 **Table 3** Effects of CO₂ concentration, inoculation, and nitrogen fertilization on total leaf area,
 521 total biomass, carbon costs to acquire nitrogen, and plant investment toward symbiotic nitrogen
 522 fixation*

		Total leaf area		Total biomass ^b		Root:shoot ratio ^a	
	df	χ^2	p	χ^2	p	χ^2	p
CO ₂	1	69.291	<0.001	131.477	<0.001	4.892	0.027
Inoculation (I)	1	35.715	<0.001	34.264	<0.001	9.790	0.002
N fertilization (N)	1	274.199	<0.001	269.046	<0.001	50.742	<0.001
CO ₂ × I	1	2.064	0.151	0.518	0.472	10.467	0.001
CO ₂ × N	1	18.655	<0.001	16.877	<0.001	0.012	0.914
I × N	1	10.804	0.001	15.779	<0.001	3.802	0.051
CO ₂ × I × N	1	<0.001	0.990	0.023	0.880	0.417	0.519

	Carbon cost to acquire nitrogen ^a		Nodule biomass: root biomass	
	χ^2	p	χ^2	p
CO ₂	76.462	<0.001	0.010	0.921
Inoculation (I)	70.846	<0.001	902.063	<0.001
N fertilization (N)	74.961	<0.001	254.741	<0.001
CO ₂ × I	33.329	<0.001	21.632	<0.001
CO ₂ × N	1.889	0.169	1.590	0.207
I × N	26.719	<0.001	132.463	<0.001
CO ₂ × I × N	6.860	0.009	2.481	0.115

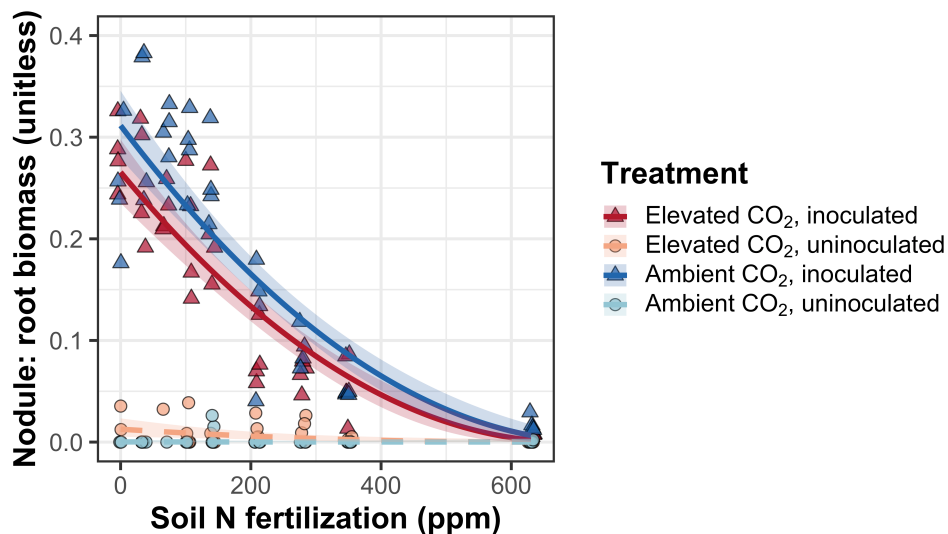
523 *Significance determined using Type II Wald χ^2 tests ($\alpha=0.05$). P-values less than 0.05 are in
 524 bold and p-values where $0.05 < p < 0.1$ are in italic font. Key: ^a=variable was natural log
 525 transformed before model fitting, ^b=variable was square root transformed before model fitting,
 526 df=degrees of freedom, χ^2 =Wald chi-square test statistic, total leaf area (cm²), total biomass (g),
 527 the ratio of root biomass to shoot biomass (unitless), belowground biomass carbon cost to
 528 acquire nitrogen (gC gN⁻¹), the ratio of root nodule biomass to root biomass (unitless)

529 **Figure 3**

530

531 **Figure 3** Effects of CO₂, nitrogen fertilization, and inoculation on total leaf area (a), total
 532 biomass (b), the ratio of root biomass to shoot biomass (c), and belowground carbon cost to
 533 acquire nitrogen (d). Nitrogen fertilization is on the x-axis in all panels. Red shaded points and
 534 trendlines indicate plants grown under elevated CO₂, while blue shaded points and trendlines
 535 indicate plants grown under ambient CO₂. Light blue and light red circular points and trendlines
 536 indicate measurements collected from uninoculated plants, while dark blue and dark red
 537 triangular points indicate measurements collected from inoculated plants. Solid trendlines
 538 indicate regression slopes that are different from zero ($p < 0.05$), while dashed trendlines indicate
 539 slopes that are not distinguishable from zero ($p > 0.05$). Error ribbons of each trendline represent
 540 the upper and lower 95% confidence intervals.

541 **Figure 4**



542

543 **Figure 4** Effects of CO₂, nitrogen fertilization, and inoculation on the ratio of root nodule
544 biomass to root biomass. Nitrogen fertilization is on the x-axis. Red shaded points and trendlines
545 indicate plants grown under elevated CO₂, while blue shaded points and trendlines indicate
546 plants grown under ambient CO₂. Light blue and light red circular points and trendlines indicate
547 measurements collected from uninoculated plants, while dark blue and dark red triangular points
548 indicate measurements collected from inoculated plants. Solid trendlines indicate regression
549 slopes that are different from zero ($p<0.05$), while dashed trendlines indicate slopes that are not
550 distinguishable from zero ($p>0.05$). Error ribbons of each trendline represent the upper and lower
551 95% confidence intervals.

552

553 **Discussion**

554 *Glycine max* plants were grown under two CO₂ concentrations, two inoculation treatments, and
555 nine nitrogen fertilization treatments in a full-factorial growth chamber experiment. We used
556 data collected from this experiment to (1) determine whether plant responses to elevated CO₂
557 aligned more closely with the nitrogen limitation or eco-evolutionary optimality hypothesis, and
558 (2) assess how the ability to associate with symbiotic nitrogen-fixing bacteria might influence
559 these responses.

560

561 *Leaf photosynthetic responses to elevated CO₂ are not related to nitrogen availability*

562 Individuals grown under elevated CO₂ experienced a reduction in $A_{\text{net},420}$, leaf nitrogen content,
563 $V_{\text{cmax}25}$, and $J_{\text{max}25}$ compared to plants grown under ambient CO₂. These patterns are consistent
564 with a downregulation of leaf-level investment toward photosynthetic enzymes, and were likely
565 driven by increased Rubisco affinity for carboxylation relative to oxygenation that decreased
566 leaf-level demand to build and maintain photosynthetic enzymes. Despite this apparent reduction
567 in leaf-level investment toward photosynthetic enzymes, elevated CO₂ increased $A_{\text{net},\text{gc}}$. This
568 response was associated with a larger reduction in $V_{\text{cmax}25}$ than $J_{\text{max}25}$, which increased $J_{\text{max}25}$:
569 $V_{\text{cmax}25}$ and allowed enhanced $A_{\text{net},\text{gc}}$ to be achieved by approaching optimal coordination (Chen
570 *et al.*, 1993; Maire *et al.*, 2012; Smith & Keenan, 2020). Additionally, the reduction in leaf
571 nitrogen content allowed increased $A_{\text{net},\text{gc}}$ to be achieved with greater photosynthetic nitrogen-use
572 efficiency. These patterns are consistent with our expectations and previous studies that have
573 investigated leaf photosynthetic responses to elevated CO₂ (Drake *et al.*, 1997; Ainsworth *et al.*,
574 2002; Ainsworth & Long, 2005; Ainsworth & Rogers, 2007; Crous *et al.*, 2010; Lee *et al.*, 2011;
575 Smith & Dukes, 2013; Poorter *et al.*, 2022; Cui *et al.*, 2023).

576 Positive effects of elevated CO₂ on $A_{\text{net},\text{gc}}$ and $J_{\text{max}25}:V_{\text{cmax}25}$ and negative effects of
577 elevated CO₂ on $A_{\text{net},420}$, $V_{\text{cmax}25}$, and $J_{\text{max}25}$ were not related to nitrogen availability, as the effects
578 of nitrogen fertilization on these traits were similar between CO₂ treatments. Instead, the increase
579 in $J_{\text{max}25}:V_{\text{cmax}25}$ and PNUE_{gc} provide strong support for the idea that leaves were downregulating
580 $V_{\text{cmax}25}$ in response to elevated CO₂ such that enhanced $A_{\text{net},\text{gc}}$ could be achieved by approaching
581 optimal coordination of Rubisco carboxylation and electron transport for RuBP regeneration
582 (Chen *et al.*, 1993; Maire *et al.*, 2012; Smith & Keenan, 2020). These responses align with
583 patterns expected from the eco-evolutionary optimality hypothesis and reinforce previous work

584 showing that leaf photosynthetic responses to elevated CO₂ are decoupled from nitrogen
585 availability (Lee *et al.*, 2011; Pastore *et al.*, 2019; Smith & Keenan, 2020; Harrison *et al.*, 2021).

586

587 *Whole-plant responses to elevated CO₂ are constrained by nitrogen availability*

588 Leaf photosynthetic responses to elevated CO₂ corresponded with increased total leaf area and
589 total biomass. These patterns were associated with an increase in the leaf mass fraction and no
590 change in stem or root mass fractions, which reduced the ratio of root biomass to shoot biomass.
591 Despite stronger aboveground allocation responses to elevated CO₂, an increase in belowground
592 carbon allocation increased the cost of acquiring nitrogen compared to plants grown under
593 ambient CO₂. Total leaf area and total biomass responses to elevated CO₂ are consistent with
594 previous studies (Ainsworth *et al.*, 2002; Ainsworth & Long, 2005; Smith & Dukes, 2013;
595 Poorter *et al.*, 2022), while increased carbon costs to acquire nitrogen follow previous work
596 suggesting that costs to acquire nitrogen increase when whole-plant demand to build new tissues
597 increases (Perkowski *et al.*, 2021). While these allocation responses to elevated CO₂ run counter
598 to our hypothesis that elevated CO₂ would increase belowground biomass more strongly than
599 aboveground biomass (Nie *et al.*, 2013; Stocker *et al.*, in review), plants grown under elevated
600 CO₂ still increased belowground carbon allocation. This response suggests that plants allocated
601 additional carbon for nutrient acquisition, likely in efforts to satisfy the greater whole-plant
602 demand to build new tissues. Regardless, priority biomass allocation to leaf tissue allowed plants
603 to experience greater primary productivity through increased total leaf area and increased $A_{net,gc}$.

604 Increasing nitrogen fertilization enhanced the positive effects of elevated CO₂ on total
605 leaf area and total biomass. Increases in belowground carbon allocation and nitrogen uptake
606 under elevated CO₂ were also enhanced with increasing nitrogen fertilization. Together, these
607 results suggest that plants grown under increased nitrogen fertilization were able to satisfy the
608 greater whole-plant demand to build new tissues and produce greater biomass under elevated
609 CO₂ by investing more strongly in nitrogen uptake. However, nitrogen fertilization did not
610 modify biomass partitioning responses to elevated CO₂, as increasing nitrogen fertilization
611 decreased the root:shoot ratio, increased the leaf and stem mass fractions, and decreased the root
612 mass fraction similarly between CO₂ treatments. Overall, these results indicate that whole-plant
613 responses to elevated CO₂ are constrained by nitrogen availability, following patterns expected
614 from the nitrogen limitation hypothesis (Luo *et al.*, 2004; Reich *et al.*, 2006; Norby *et al.*, 2010).

615 However, nitrogen availability did not modify whether plants invested in aboveground or
616 belowground tissues, indicating that biomass allocation responses to elevated CO₂ were more
617 strongly dictated by changes in whole-plant demand to build new tissues than the supply of
618 nutrients.

619

620 *Inoculation does not affect leaf or whole-plant responses to elevated CO₂*
621 Inoculation increased N_{area} , $A_{\text{net},420}$, $A_{\text{net,gc}}$, $V_{\text{cmax}25}$, $J_{\text{max}25}$, total leaf area, and total biomass, and
622 decreased $J_{\text{max}25}:V_{\text{cmax}25}$. These patterns support previous literature suggesting that species that
623 form associations with symbiotic nitrogen-fixing bacteria have increased leaf nitrogen content,
624 photosynthetic capacity, and growth compared to species that do not form such associations
625 (Adams *et al.*, 2016; Bytnerowicz *et al.*, 2023). Positive effects of inoculation on leaf and whole-
626 plant traits were most apparent under low nitrogen fertilization and diminished with increasing
627 nitrogen fertilization as plant investment in symbiotic nitrogen fixation decreased. These patterns
628 provide another line of support for the idea that the ability to associate with symbiotic nitrogen-
629 fixing bacteria may confer competitive benefits in low soil nitrogen environments (Rastetter *et*
630 *al.*, 2001; Andrews *et al.*, 2011; McCulloch & Porder, 2021), although recent work highlights
631 that plants can still fix nitrogen in high soil nitrogen environments (Menge *et al.*, 2023).

632 Elevated CO₂ increased root nodule biomass in inoculated plants, following our
633 expectation that increased whole-plant demand to build new tissues would increase nitrogen
634 uptake through symbiotic nitrogen fixation. However, stronger increases in root biomass than
635 root nodulation under elevated CO₂ indicate that plants may have invested more strongly toward
636 less costly direct uptake pathways as demand to build and maintain new tissues increased. If true,
637 these patterns contrast previous work showing that relative plant investment toward symbiotic
638 nitrogen fixation tends to be greater under scenarios that increase whole-plant demand to acquire
639 nitrogen (Taylor & Menge, 2018; Friel & Friesen, 2019; McCulloch & Porder, 2021; Perkowski
640 *et al.*, 2021). However, this allocation response may alternatively indicate that plants were
641 allocating relatively more biomass toward root tissues in order to acquire soil resources other
642 than nitrogen, as increased nitrogen uptake through symbiotic nitrogen fixation may increase the
643 extent by which leaf and whole-plant physiology becomes limited other nutrients, such as
644 phosphorus (Finzi & Rodgers, 2009).

645 Despite increased root nodulation, the effects of elevated CO₂ on V_{cmax25} , J_{max25} ,
646 J_{max25} : V_{cmax25} , total leaf area, and total biomass were not modified by inoculation treatment.
647 These patterns suggest that ability to associate with symbiotic nitrogen-fixing bacteria did not
648 modify whether leaf or whole-plant responses to elevated CO₂ were driven by patterns expected
649 through either the nitrogen limitation or eco-evolutionary optimality hypothesis, even when
650 plants increased nitrogen uptake through symbiotic nitrogen fixation. We observed these patterns
651 regardless of nitrogen fertilization level, which contrasted our hypothesis that inoculation would
652 exert stronger effects on plant responses to elevated CO₂ under low nitrogen fertilization.

653

654 *Modeling implications*

655 Many terrestrial biosphere models predict photosynthetic capacity through parameterized
656 relationships between N_{area} and V_{cmax} (Smith & Dukes, 2013; Rogers *et al.*, 2017), which assumes
657 that leaf nitrogen-photosynthesis relationships are constant across growing environments. Our
658 results build on previous work suggesting that leaf nitrogen-photosynthesis relationships
659 dynamically change across growing environments (Luo *et al.*, 2021; Waring *et al.*, 2023).
660 Specifically, elevated CO₂ reduced leaf nitrogen content more strongly than it increased $A_{net,gc}$
661 and decreased V_{cmax25} and J_{max25} , while inoculation increased V_{cmax25} and J_{max25} more strongly
662 than it increased N_{area} . These patterns indicate that elevated CO₂ increased the fractional pool of
663 leaf nitrogen content allocated to Rubisco and bioenergetics, while inoculation decreased the
664 fraction of leaf nitrogen content allocated to Rubisco and bioenergetics (Niinemets & Tenhunen,
665 1997). Additionally, the positive effect of increasing nitrogen fertilization on apparent
666 photosynthetic capacity was only observed in uninoculated plants, as increasing nitrogen
667 fertilization did not affect V_{cmax25} or J_{max25} in inoculated plants. The positive effect of increasing
668 nitrogen fertilization on N_{area} and Chl_{area} was also markedly weaker in inoculated plants than in
669 uninoculated plants. These patterns indicate that leaf nitrogen-photosynthesis relationships are
670 context-dependent on nitrogen acquisition strategy, may only be constant in environments where
671 nitrogen availability limits leaf physiology, and will likely shift in response to increasing
672 atmospheric CO₂ concentrations. Terrestrial biosphere models that predict photosynthetic
673 capacity through parameterized relationships between N_{area} and V_{cmax} (Kattge *et al.*, 2009;
674 Walker *et al.*, 2014) may risk overestimating photosynthetic capacity, therefore net primary
675 productivity and the magnitude of the land carbon sink, under future novel growth environments.

676 Our results demonstrate that optimal resource allocation to photosynthetic capacity
677 defines leaf photosynthetic responses to elevated CO₂ and that these responses are not modified
678 by nitrogen availability. Current approaches for simulating photosynthetic responses to CO₂ in
679 terrestrial biosphere models with coupled carbon and nitrogen cycles often invoke patterns
680 expected from nitrogen limitation, where nitrogen availability diminishes with time due to
681 increasing CO₂ concentrations because whole-plant nitrogen demand continually exceeds supply,
682 depleting the pool of available nitrogen for plants to acquire and allocate to the construction and
683 maintenance of new tissues. This response causes models to simulate a reduction in leaf nitrogen
684 content and therefore photosynthetic capacity, as leaf-level photosynthesis is commonly modeled
685 as a function of positive relationships between nitrogen availability, leaf nitrogen content, and
686 photosynthetic capacity (Smith & Dukes, 2013; Rogers *et al.*, 2017). Findings presented here
687 contradict this framework, suggesting that leaf photosynthetic responses to elevated CO₂ result in
688 optimized nitrogen allocation to satisfy reduced leaf nitrogen demand to build and maintain
689 photosynthetic enzymes. Optimality models that use principles from optimal coordination and
690 photosynthetic least-cost theories are capable of capturing photosynthetic responses to CO₂
691 independent of nitrogen availability (Smith & Keenan, 2020; Harrison *et al.*, 2021), suggesting
692 that the inclusion of such frameworks may improve the accuracy by which terrestrial biosphere
693 models simulate photosynthetic processes with increasing atmospheric CO₂ concentrations.
694

695 *Limitations*

696 Previous work has highlighted that pot experiments restrict belowground rooting volume and
697 may alter plant allocation responses to environmental change (Ainsworth *et al.*, 2002; Poorter *et*
698 *al.*, 2012). In this study, the ratio of pot volume to total biomass was greater under elevated CO₂
699 and increased with increasing nitrogen fertilization such that several treatment combinations
700 exceeded values recommended to avoid growth limitation imposed by pot volume (<1 g L⁻¹;
701 Table S7; Fig. S7) (Poorter *et al.* 2012). However, there was no evidence to suggest that pot size
702 limited plant growth, as evidenced by the lack of a saturating effect of increasing fertilization on
703 total biomass, belowground carbon biomass, or root biomass under conditions where biomass:
704 pot volume ratios exceeded 1 g L⁻¹ (e.g., individuals of either inoculation status grown under
705 high fertilization and elevated CO₂). Field studies that do not restrict belowground rooting
706 volume have observed similar leaf and whole-plant responses to elevated CO₂ (Crous *et al.* 2010;

707 Lee et al. 2011; Pastore et al. 2019; Smith & Keenan 2020), indicating that the pot volume used
708 in this study (6 L) was sufficient to avoid growth limitation. However, a similar experiment
709 conducted under field conditions would be helpful for validating the patterns observed here.

710

711 *Conclusions*

712 Our study provides strong support for the eco-evolutionary optimality hypothesis at the leaf
713 level, where leaf photosynthetic responses to elevated CO₂ were independent of nitrogen
714 fertilization and inoculation treatment. Instead, elevated CO₂ reduced the maximum rate of
715 Rubisco carboxylation more strongly than it reduced the maximum rate of electron transport for
716 RuBP regeneration, allowing plants to achieve greater net photosynthesis rates under CO₂
717 growth conditions by approaching optimal coordination while simultaneously reducing leaf
718 nitrogen demand to build and maintain photosynthetic enzymes. In contrast, at the whole-plant
719 level, nitrogen availability played a central role in regulating plant responses to elevated CO₂,
720 consistent with the nitrogen limitation hypothesis. Specifically, increases in total leaf area, total
721 biomass, and plant nitrogen under elevated CO₂ were all enhanced with increasing nitrogen
722 fertilization. While inoculation increased root nodulation under elevated CO₂, it did not
723 significantly enhance whole-plant responses to elevated CO₂, even under low nitrogen conditions
724 where plants were most strongly invested in symbiotic nitrogen-fixing bacteria. This response
725 may have been due to stronger increases in root biomass that caused plants to prioritize direct
726 nitrogen uptake pathways over symbiotic nitrogen fixation as whole-plant demand to build new
727 tissues increased. Overall, results indicate that plants grown under elevated CO₂ responded to
728 increased nitrogen availability by increasing the number of optimally coordinated leaves, and
729 changes in nitrogen availability did not modify the downregulation in apparent photosynthetic
730 capacity under elevated CO₂. The differential role of nitrogen availability on leaf and whole-
731 plant responses to elevated CO₂ and the dynamic leaf nitrogen-photosynthesis relationships
732 across CO₂ and nitrogen fertilization treatments suggests that terrestrial biosphere models may
733 improve simulations of photosynthetic responses to increasing atmospheric CO₂ concentrations
734 by adopting frameworks that include optimality principles.

735

736 **Conflicts of Interest**

737 The authors declare no conflicts of interest.

738

739 **Acknowledgements**

740 This study is a contribution to the LEMONTREE (Land Ecosystem Models based On New
741 Theory, obseRvations and ExperimEnts) project, receiving support through Schmidt Sciences,
742 LLC. EAP acknowledges support from a Texas Tech University Doctoral Dissertation
743 Completion Fellowship and a Botanical Society of America Graduate Student Research Award.
744 This work was also supported by US National Science Foundation awards to NGS (DEB-
745 2045968 and DEB-2217353).

746

747 **Data Availability**

748 All R scripts, data, and metadata are available at <https://doi.org/10.5281/zenodo.12812758> (or on
749 GitHub at: https://github.com/eaperkowski/NxCO2xI_ms_data)

750

751 **Author contributions**

752 EAP conceptualized the study objectives and designed the experiment in collaboration with
753 NGS, collected data, conducted data analysis, and wrote the first manuscript draft. EE assisted
754 with data collection and experiment maintenance. NGS conceptualized study objectives and
755 experimental design with EAP and oversaw experiment progress. All authors provided
756 manuscript feedback and approved the manuscript in its current form for submission to *Plant,*
757 *Cell & Environment.*

758

759 **References**

- 760 **Adams MA, Turnbull TL, Sprent JI, Buchmann N. 2016.** Legumes are different: Leaf
761 nitrogen, photosynthesis, and water use efficiency. *Proceedings of the National Academy of
762 Sciences of the United States of America* **113:** 4098–4103.
- 763 **Ainsworth EA, Davey PA, Bernacchi CJ, Dermody OC, Heaton EA, Moore DJP, Morgan
764 PB, Naidu SL, Ra HSY, Zhu XG, et al. 2002.** A meta-analysis of elevated [CO₂] effects on
765 soybean (*Glycine max*) physiology, growth and yield. *Global Change Biology* **8:** 695–709.
- 766 **Ainsworth EA, Long SP. 2005.** What have we learned from 15 years of free-air CO₂ enrichment
767 (FACE)? A meta-analytic review of the responses of photosynthesis, canopy properties and plant
768 production to rising CO₂. *New Phytologist* **165:** 351–372.

- 769 **Ainsworth EA, Rogers A.** 2007. The response of photosynthesis and stomatal conductance to
770 rising [CO₂]: mechanisms and environmental interactions. *Plant, Cell & Environment* **30**: 258–
771 270.
- 772 **Allen K, Fisher JB, Phillips RP, Powers JS, Brzostek ER.** 2020. Modeling the carbon cost of
773 plant nitrogen and phosphorus uptake across temperate and tropical forests. *Frontiers in Forests*
774 and Global Change
- 775 **Andrews M, James EK, Sprent JI, Boddey RM, Gross E, dos Reis FB.** 2011. Nitrogen
776 fixation in legumes and actinorhizal plants in natural ecosystems: Values obtained using ¹⁵N
777 natural abundance. *Plant Ecology and Diversity* **4**: 117–130.
- 778 **Arora VK, Katavouta A, Williams RG, Jones CD, Brovkin V, Friedlingstein P, Schwinger
779 J, Bopp L, Boucher O, Cadule P, et al.** 2020. Carbon-concentration and carbon-climate
780 feedbacks in CMIP6 models and their comparison to CMIP5 models. *Biogeosciences* **17**: 4173–
781 4222.
- 782 **Barber SA.** 1962. A diffusion and mass-flow concept of soil nutrient availability. *Soil Science*
783 **93**: 39–49.
- 784 **Barnes JD, Balaguer L, Manrique E, Elvira S, Davison AW.** 1992. A reappraisal of the use of
785 DMSO for the extraction and determination of chlorophylls a and b in lichens and higher plants.
786 *Environmental and Experimental Botany* **32**: 85–100.
- 787 **Bates D, Mächler M, Bolker B, Walker S.** 2015. Fitting linear mixed-effects models using
788 lme4. *Journal of Statistical Software* **67**: 1–48.
- 789 **Bazzaz FA.** 1990. The response of natural ecosystems to the rising global CO₂ levels. *Annual
790 Review of Ecology and Systematics* **21**: 167–196.
- 791 **Bernacchi CJ, Morgan PB, Ort DR, Long SP.** 2005. The growth of soybean under free air
792 [CO₂] enrichment (FACE) stimulates photosynthesis while decreasing in vivo Rubisco capacity.
793 *Planta* **220**: 434–446.
- 794 **Bernacchi CJ, Singsaas EL, Pimentel C, Portis AR, Long SP.** 2001. Improved temperature
795 response functions for models of Rubisco-limited photosynthesis. *Plant, Cell and Environment*
796 **24**: 253–259.
- 797 **Brzostek ER, Fisher JB, Phillips RP.** 2014. Modeling the carbon cost of plant nitrogen
798 acquisition: Mycorrhizal trade-offs and multipath resistance uptake improve predictions of
799 retranslocation. *Journal of Geophysical Research: Biogeosciences* **119**: 1684–1697.

- 800 **Bytnerowicz TA, Funk JL, Menge DNL, Perakis SS, Wolf AA.** 2023. Leaf nitrogen affects
801 photosynthesis and water use efficiency similarly in nitrogen-fixing and non-fixing trees. *Journal*
802 *of Ecology*: 1–15.
- 803 **Chen J-L, Reynolds JF, Harley PC, Tenhunen JD.** 1993. Coordination theory of leaf nitrogen
804 distribution in a canopy. *Oecologia* **93**: 63–69.
- 805 **Coleman JS, McConaughay KDM, Bazzaz FA.** 1993. Elevated CO₂ and plant nitrogen-use:
806 is reduced tissue nitrogen concentration size-dependent? *Oecologia* **93**: 195–200.
- 807 **Crous KY, Reich PB, Hunter MD, Ellsworth DS.** 2010. Maintenance of leaf N controls the
808 photosynthetic CO₂ response of grassland species exposed to 9 years of free-air CO₂ enrichment.
809 *Global Change Biology* **16**: 2076–2088.
- 810 **Cui E, Xia J, Luo Y.** 2023. Nitrogen use strategy drives interspecific differences in plant
811 photosynthetic CO₂ acclimation. *Global Change Biology* **29**: 3667–3677.
- 812 **Curtis PS.** 1996. A meta-analysis of leaf gas exchange and nitrogen in trees grown under
813 elevated carbon dioxide. *Plant, Cell and Environment* **19**: 127–137.
- 814 **Davies-Barnard T, Meyerholt J, Zaehle S, Friedlingstein P, Brovkin V, Fan Y, Fisher RA,**
815 **Jones CD, Lee H, Peano D, et al.** 2020. Nitrogen cycling in CMIP6 land surface models:
816 progress and limitations. *Biogeosciences* **17**: 5129–5148.
- 817 **Davies-Barnard T, Zaehle S, Friedlingstein P.** 2022. Assessment of the impacts of biological
818 nitrogen fixation structural uncertainty in CMIP6 earth system models. *Biogeosciences* **19**:
819 3491–3503.
- 820 **Dong N, Wright IJ, Chen JM, Luo X, Wang H, Keenan TF, Smith NG, Prentice IC.** 2022.
821 Rising CO₂ and warming reduce global canopy demand for nitrogen. *New Phytologist* **235**:
822 1692–1700.
- 823 **Drake BG, González-Meler MA, Long SP.** 1997. More efficient plants: a consequence of
824 rising atmospheric CO₂? *Annual Review of Plant Biology* **48**: 609–639.
- 825 **Duursma RA.** 2015. Plantcophys - an R package for analysing and modelling leaf gas
826 exchange data. *PLOS ONE* **10**: e0143346.
- 827 **Evans JR.** 1989. Photosynthesis and nitrogen relationships in leaves of C₃ plants. *Oecologia* **78**:
828 9–19.
- 829 **Evans JR, Clarke VC.** 2019. The nitrogen cost of photosynthesis. *Journal of Experimental*
830 *Botany* **70**: 7–15.

- 831 **Farquhar GD, von Caemmerer S, Berry JA.** 1980. A biochemical model of photosynthetic
832 CO₂ assimilation in leaves of C₃ species. *Planta* **149**: 78–90.
- 833 **Finzi AC, Moore DJP, DeLucia EH, Lichter J, Hofmockel KS, Jackson RB, Kim HS,**
834 **Matamala R, McCarthy HR, Oren R, et al.** 2006. Progressive nitrogen limitation of ecosystem
835 processes under elevated CO₂ in a warm-temperate forest. *Ecology* **87**: 15–25.
- 836 **Finzi AC, Norby RJ, Calfapietra C, Gallet-Budynek A, Gielen B, Holmes WE, Hoosbeek**
837 **MR, Iversen CM, Jackson RB, Kubiske ME, et al.** 2007. Increases in nitrogen uptake rather
838 than nitrogen-use efficiency support higher rates of temperate forest productivity under elevated
839 CO₂. *Proceedings of the National Academy of Sciences* **104**: 14014–14019.
- 840 **Finzi AC, Rodgers VL.** 2009. Bottom-up rather than top-down processes regulate the
841 abundance and activity of nitrogen fixing plants in two Connecticut old-field ecosystems.
842 *Biogeochemistry* **95**: 309–321.
- 843 **Fisher JB, Sitch S, Malhi Y, Fisher RA, Huntingford C, Tan S-Y.** 2010. Carbon cost of plant
844 nitrogen acquisition: A mechanistic, globally applicable model of plant nitrogen uptake,
845 retranslocation, and fixation. *Global Biogeochemical Cycles* **24**: 1–17.
- 846 **Fox J, Weisberg S.** 2019. *An R companion to applied regression*. Thousand Oaks, California:
847 Sage.
- 848 **Friedlingstein P, Meinshausen M, Arora VK, Jones CD, Anav A, Liddicoat SK, Knutti R.**
849 2014. Uncertainties in CMIP5 climate projections due to carbon cycle feedbacks. *Journal of*
850 *Climate* **27**: 511–526.
- 851 **Friel CA, Friesen ML.** 2019. Legumes modulate allocation to rhizobial nitrogen fixation in
852 response to factorial light and nitrogen manipulation. *Frontiers in Plant Science* **10**: 1316.
- 853 **Gutschick VP.** 1981. Evolved strategies in nitrogen acquisition by plants. *The American*
854 *Naturalist* **118**: 607–637.
- 855 **Harrison SP, Cramer W, Franklin O, Prentice IC, Wang H, Bränström Å, de Boer H,**
856 **Dieckmann U, Joshi J, Keenan TF, et al.** 2021. Eco-evolutionary optimality as a means to
857 improve vegetation and land-surface models. *New Phytologist* **231**: 2125–2141.
- 858 **Hoagland DR, Arnon DI.** 1950. The water-culture method for growing plants without soil.
859 *California Agricultural Experiment Station*: 347 **347**: 1–32.
- 860 **Hungate BA, Dukes JS, Shaw MR, Luo Y, Field CB.** 2003. Nitrogen and climate change.
861 *Science* **302**: 1512–1513.

- 862 **IPCC.** 2021. *Climate Change 2021: The Physical Science Basis. Contribution of Working Group*
863 *I to the Sixth Assessment Report of the Intergovernmental Panel on Climate Change* (V Masson-
864 Delmotte, P Zhai, A Pirani, SL Connors, S Berger, N Caud, Y Chen, L Goldfarb, MI Gomis, M
865 Huang, *et al.*, Eds.). Cambridge, UK and New York, USA: Cambridge University Press.
- 866 **Katabuchi M.** 2015. LeafArea: An R package for rapid digital analysis of leaf area. *Ecological*
867 *Research* **30**: 1073–1077.
- 868 **Kattge J, Knorr W, Raddatz T, Wirth C.** 2009. Quantifying photosynthetic capacity and its
869 relationship to leaf nitrogen content for global-scale terrestrial biosphere models. *Global Change*
870 *Biology* **15**: 976–991.
- 871 **Kenward MG, Roger JH.** 1997. Small sample inference for fixed effects from restricted
872 maximum likelihood. *Biometrics* **53**: 983.
- 873 **Kou-Giesbrecht S, Arora VK, Seiler C, Arneth A, Falk S, Jain AK, Joos F, Kennedy D,**
874 **Knauer J, Sitch S, et al.** 2023. Evaluating nitrogen cycling in terrestrial biosphere models: a
875 disconnect between the carbon and nitrogen cycles. *Earth System Dynamics* **14**: 767–795.
- 876 **LeBauer DS, Treseder KK.** 2008. Nitrogen limitation of net primary productivity in terrestrial
877 ecosystems is globally distributed. *Ecology* **89**: 371–379.
- 878 **Lee TD, Barrott SH, Reich PB.** 2011. Photosynthetic responses of 13 grassland species across
879 11 years of free-air CO₂ enrichment is modest, consistent and independent of N supply. *Global*
880 *Change Biology* **17**: 2893–2904.
- 881 **Lenth R.** 2019. emmeans: estimated marginal means, aka least-squares means.
- 882 **Liang J, Qi X, Souza L, Luo Y.** 2016. Processes regulating progressive nitrogen limitation
883 under elevated carbon dioxide: a meta-analysis. *Biogeosciences* **13**: 2689–2699.
- 884 **Lu J, Yang J, Keitel C, Yin L, Wang P, Cheng W, Dijkstra FA.** 2022. Belowground carbon
885 efficiency for nitrogen and phosphorus acquisition varies between *Lolium perenne* and *Trifolium*
886 *repens* and depends on phosphorus fertilization. *Frontiers in Plant Science* **13**: 1–9.
- 887 **Luo Y, Currie WS, Dukes JS, Finzi AC, Hartwig UA, Hungate BA, McMurtrie RE, Oren**
888 **R, Parton WJ, Pataki DE, et al.** 2004. Progressive nitrogen limitation of ecosystem responses
889 to rising atmospheric carbon dioxide. *BioScience* **54**: 731–739.
- 890 **Luo Y, Field CB, Mooney HA.** 1994. Predicting responses of photosynthesis and root fraction
891 to elevated [CO₂]: interactions among carbon, nitrogen, and growth. *Plant, Cell & Environment*
892 **17**: 1195–1204.

- 893 **Luo X, Keenan TF, Chen JM, Croft H, Prentice IC, Smith NG, Walker AP, Wang H, Wang**
894 **R, Xu C, et al.** 2021. Global variation in the fraction of leaf nitrogen allocated to photosynthesis.
895 *Nature Communications* **12**: 4866.
- 896 **Maire V, Martre P, Kattge J, Gastal F, Esser G, Fontaine S, Soussana J-F.** 2012. The
897 coordination of leaf photosynthesis links C and N fluxes in C₃ plant species. *PLoS ONE* **7**:
898 e38345.
- 899 **Makino A, Harada M, Sato T, Nakano H, Mae T.** 1997. Growth and N allocation in rice
900 plants under CO₂ enrichment. *Plant Physiology* **115**: 199–203.
- 901 **McCulloch LA, Porder S.** 2021. Light fuels while nitrogen suppresses symbiotic nitrogen
902 fixation hotspots in neotropical canopy gap seedlings. *New Phytologist* **231**: 1734–1745.
- 903 **Medlyn BE, Badeck FW, De Pury DGG, Barton CVM, Broadmeadow M, Ceulemans R, de**
904 **Angelis P, Forstreuter M, Jach ME, Kellomäki S, et al.** 1999. Effects of elevated [CO₂] on
905 photosynthesis in European forest species: A meta-analysis of model parameters. *Plant, Cell and*
906 *Environment* **22**: 1475–1495.
- 907 **Menge DNL, Wolf AA, Funk JL, Perakis SS, Akana PR, Arkebauer R, Bytnerowicz TA,**
908 **Carreras Pereira KA, Huddell AM, Kou-Giesbrecht S, et al.** 2023. Tree symbioses sustain
909 nitrogen fixation despite excess nitrogen supply. *Ecological Monographs* **93**: 1–27.
- 910 **Meyerholt J, Sickel K, Zaehle S.** 2020. Ensemble projections elucidate effects of uncertainty in
911 terrestrial nitrogen limitation on future carbon uptake. *Global Change Biology* **26**: 3978–3996.
- 912 **Moore DJP, Aref S, Ho RM, Pippen JS, Hamilton JG, De Lucia EH.** 2006. Annual basal area
913 increment and growth duration of *Pinus taeda* in response to eight years of free-air carbon
914 dioxide enrichment. *Global Change Biology* **12**: 1367–1377.
- 915 **Nakano H, Makino A, Mae T.** 1997. The effect of elevated partial pressures of CO₂ on the
916 relationship between photosynthetic capacity and N content in rice leaves. *Plant Physiology* **115**:
917 191–198.
- 918 **Nie M, Lu M, Bell J, Raut S, Pendall E.** 2013. Altered root traits due to elevated CO₂: A meta-
919 analysis. *Global Ecology and Biogeography* **22**: 1095–1105.
- 920 **Niinemets Ü, Tenhunen JD.** 1997. A model separating leaf structural and physiological effects
921 on carbon gain along light gradients for the shade-tolerant species *Acer saccharum*. *Plant, Cell*
922 *and Environment* **20**: 845–866.

- 923 **Norby RJ, Warren JM, Iversen CM, Medlyn BE, McMurtrie RE.** 2010. CO₂ enhancement
924 of forest productivity constrained by limited nitrogen availability. *Proceedings of the National
925 Academy of Sciences* **107**: 19368–19373.
- 926 **Pastore MA, Lee TD, Hobbie SE, Reich PB.** 2019. Strong photosynthetic acclimation and
927 enhanced water-use efficiency in grassland functional groups persist over 21 years of CO₂
928 enrichment, independent of nitrogen supply. *Global Change Biology* **25**: 3031–3044.
- 929 **Peng Y, Prentice IC, Bloomfield KJ, Campioli M, Guo Z, Sun Y, Tian D, Wang X, Vicca S,
930 Stocker BD.** 2023. Global terrestrial nitrogen uptake and nitrogen use efficiency. *Journal of
931 Ecology*: 1–18.
- 932 **Perkowski EA, Waring EF, Smith NG.** 2021. Root mass carbon costs to acquire nitrogen are
933 determined by nitrogen and light availability in two species with different nitrogen acquisition
934 strategies. *Journal of Experimental Botany* **72**: 5766–5776.
- 935 **Poorter H, Böhler J, Van Dusschoten D, Climent J, Postma JA.** 2012. Pot size matters: A
936 meta-analysis of the effects of rooting volume on plant growth. *Functional Plant Biology* **39**:
937 839–850.
- 938 **Poorter H, Knopf O, Wright IJ, Temme AA, Hogewoning SW, Graf A, Cernusak LA, Pons
939 TL.** 2022. A meta-analysis of responses of C₃ plants to atmospheric CO₂: dose–response curves
940 for 85 traits ranging from the molecular to the whole-plant level. *New Phytologist* **233**: 1560–
941 1596.
- 942 **Prentice IC, Dong N, Gleason SM, Maire V, Wright IJ.** 2014. Balancing the costs of carbon
943 gain and water transport: testing a new theoretical framework for plant functional ecology.
944 *Ecology Letters* **17**: 82–91.
- 945 **Prentice IC, Liang X, Medlyn BE, Wang Y-P.** 2015. Reliable, robust and realistic: The three
946 R's of next-generation land-surface modelling. *Atmospheric Chemistry and Physics* **15**: 5987–
947 6005.
- 948 **R Core Team.** 2021. R: A language and environment for statistical computing.
- 949 **Rastetter EB, Vitousek PM, Field CB, Shaver GR, Herbert D, Ågren GI.** 2001. Resource
950 optimization and symbiotic nitrogen fixation. *Ecosystems* **4**: 369–388.
- 951 **Reich PB, Hobbie SE, Lee TD, Ellsworth DS, West JB, Tilman D, Knops JMH, Naeem S,
952 Trost J.** 2006. Nitrogen limitation constrains sustainability of ecosystem response to CO₂.
953 *Nature* **440**: 922–925.

- 954 **Rogers A, Medlyn BE, Dukes JS, Bonan GB, Caemmerer S, Dietze MC, Kattge J, Leakey**
955 **ADB, Mercado LM, Niinemets Ü, et al.** 2017. A roadmap for improving the representation of
956 photosynthesis in Earth system models. *New Phytologist* **213**: 22–42.
- 957 **Saathoff AJ, Welles J.** 2021. Gas exchange measurements in the unsteady state. *Plant Cell and*
958 *Environment* **44**: 3509–3523.
- 959 **Schneider CA, Rasband WS, Eliceiri KW.** 2012. NIH Image to ImageJ: 25 years of image
960 analysis. *Nature Methods* **9**: 671–675.
- 961 **Smith NG, Dukes JS.** 2013. Plant respiration and photosynthesis in global-scale models:
962 incorporating acclimation to temperature and CO₂. *Global Change Biology* **19**: 45–63.
- 963 **Smith NG, Keenan TF.** 2020. Mechanisms underlying leaf photosynthetic acclimation to
964 warming and elevated CO₂ as inferred from least-cost optimality theory. *Global Change Biology*
965 **26**: 5202–5216.
- 966 **Smith NG, Keenan TF, Prentice IC, Wang H, Wright IJ, Niinemets Ü, Crous KY,**
967 **Domingues TF, Guerrieri R, Ishida FY, et al.** 2019. Global photosynthetic capacity is
968 optimized to the environment. *Ecology Letters* **22**: 506–517.
- 969 **Smith SE, Read DJ.** 2008. *Mycorrhizal Symbiosis*.
- 970 **Stocker BD, Dong N, Perkowski EA, Schneider PD, Xu H, de Boer H, Rebel KT, Smith NG,**
971 **Van Sundert K, Wang H, et al.** Empirical evidence and theoretical understanding of ecosystem
972 carbon and nitrogen interactions. *in review*.
- 973 **Taylor BN, Menge DNL.** 2018. Light regulates tropical symbiotic nitrogen fixation more
974 strongly than soil nitrogen. *Nature Plants* **4**: 655–661.
- 975 **Tejera-Nieves M, Seong DY, Reist L, Walker BJ.** 2024. The Dynamic Assimilation Technique
976 measures photosynthetic CO₂ response curves with similar fidelity to steady-state approaches in
977 half the time. *Journal of Experimental Botany* **0**: 1–22.
- 978 **Terrer C, Vicca S, Stocker BD, Hungate BA, Phillips RP, Reich PB, Finzi AC, Prentice IC.**
979 **2018.** Ecosystem responses to elevated CO₂ governed by plant–soil interactions and the cost of
980 nitrogen acquisition. *New Phytologist* **217**: 507–522.
- 981 **Vitousek PM, Howarth RW.** 1991. Nitrogen limitation on land and in the sea: How can it
982 occur? *Biogeochemistry* **13**: 87–115.
- 983 **Walker AP, Beckerman AP, Gu L, Kattge J, Cernusak LA, Domingues TF, Scales JC,**
984 **Wohlfahrt G, Wullschleger SD, Woodward FI.** 2014. The relationship of leaf photosynthetic

- 985 traits - V_{cmax} and J_{max} - to leaf nitrogen, leaf phosphorus, and specific leaf area: a meta-analysis
986 and modeling study. *Ecology and Evolution* **4**: 3218–3235.
- 987 **Wang H, Prentice IC, Keenan TF, Davis TW, Wright IJ, Cornwell WK, Evans BJ, Peng C.**
988 **2017.** Towards a universal model for carbon dioxide uptake by plants. *Nature Plants* **3**: 734–741.
- 989 **Waring EF, Perkowski EA, Smith NG. 2023.** Soil nitrogen fertilization reduces relative leaf
990 nitrogen allocation to photosynthesis. *Journal of Experimental Botany* **74**: 5166–5180.
- 991 **Wellburn AR. 1994.** The spectral determination of chlorophylls a and b, as well as total
992 carotenoids, using various solvents with spectrophotometers of different resolution. *Journal of*
993 *Plant Physiology* **144**: 307–313.
- 994 **Wieder WR, Cleveland CC, Smith WK, Todd-Brown K. 2015.** Future productivity and
995 carbon storage limited by terrestrial nutrient availability. *Nature Geoscience* **8**: 441–444.
- 996 **Wright IJ, Reich PB, Westoby M. 2003.** Least-cost input mixtures of water and nitrogen for
997 photosynthesis. *The American Naturalist* **161**: 98–111.
- 998